Research Square

Preprints are preliminary reports that have not undergone peer review.
They should not be considered conclusive, used to inform clinical practice,
or referenced by the media as validated information.

Toward a Perfect Lens: Automated Design of GRIN Double-Freeform Systems for Broadband Aberration and Chromaticity Correction

Donglin Ma

madonglin@hust.edu.cn

Huazhong University of Science and Technology https://orcid.org/0000-0001-5129-7770

Rongqi Shang

Huazhong University of Science and Technology

Article

Keywords: Symplectic geometry, Dragt-Finn factorization, Extended phase space, Gradient-index (GRIN) media, Freeform optics

Posted Date: November 10th, 2026

DOI: https://doi.org/10.21203/rs.3.rs-9332818/v1

License: This work is licensed under a Creative Commons Attribution 4.0 International License.
Read Full License

Additional Declarations: There is no conflict of interest

Toward a Perfect Lens: Automated Design of GRIN Double-Freeform Systems for Broadband Aberration and Chromaticity Correction

Rongqi Shang[1], Donglin Ma[2,**]

[1] School of Optical and Electronic Information, Huazhong University of Science and Technology, Wuhan, Hubei 430074, China

Email: m202470016@hust.edu.cn

[2] School of Optical and Electronic Information, Huazhong University of Science and Technology, Wuhan, Hubei 430074, China

Email: madonglin@hust.edu.cn

Abstract

In conventional optical design, the inability of a single lens to simultaneously correct high-order geometric and chromatic aberrations over a broad spectral range constitutes a persistent physical bottleneck limiting the development of ultracompact imaging systems. This limitation fundamentally arises from the severely restricted degrees of freedom associated with traditional lenses, which rely solely on interfacial modulation, combined with the intrinsic dispersion of homogeneous media. In this paper, we propose a global inverse design framework based on gradient-index (GRIN) dual-freeform optics to overcome the physical constraints of single-lens imaging. By introducing an extended phase space that incorporates wavelength, the complex ray-tracing evolution is rigorously transformed into an analytical algebraic reconstruction process. Based on this framework, a physical mechanism for chromatic aberration compensation is revealed: exploiting the three-dimensional "spatial dispersion gradient" within the GRIN medium induces an anomalous negative chromatic aberration effect, which globally and precisely cancels the intrinsic positive chromatic aberration introduced by freeform refractions. As a methodological validation, an objective singlet lens with highly demanding performance parameters (a half field of view up to 50°) is inversely designed. Quantitative evaluations demonstrate that across the entire visible spectrum, the full-field root-mean-square (RMS) spot radius is strictly controlled to within 8 nm, achieving broadband aberration-free and achromatic imaging with geometrical spot sizes well within the diffraction limit. This work provides a rigorous theoretical methodology and an implementable pathway for the design of ultracompact imaging optics, while substantially reducing the reliance on manual experience and iterative numerical optimization in advanced freeform optical design.

**Corresponding author: madonglin@hust.edu.cn; Tel: +86-18627924296

Keywords: Symplectic geometry, Dragt-Finn factorization, Extended phase space, Gradient-index (GRIN) media, Freeform optics

1 Introduction

The analysis and correction of optical aberrations span the entire workflow of optical system design, representing a core intersection of classical mechanics, differential geometry, and modern optics. From Hamilton's formulation of the optical characteristic function theory[1] to Seidel's establishment of the third-order aberration algebraic system,[2] the theoretical development of geometrical optics has continually revolved around extracting analytically resolvable aberration laws from complex ray mapping relationships.[3] In recent years, the rapid iteration of portable optoelectronic devices,[4–8] along with the development of advanced astronomical observatories requiring high-efficiency, multi-spectrum compact integration,[9] has imposed extreme performance demands on modern optical systemsrequiring large fields of view, ultracompact form factors, and broadband imaging capabilities. This pushes optical design continuously toward its theoretical limits. However, when a system must simultaneously achieve large-FOV and broadband imaging, traditional aberration theories and design methodologies exhibit insurmountable limitations in both physical realizability and mathematical convergence. As early as 2005, *Science* listed "Can we make a perfect optical lens?" as one of the 125 most challenging global scientific questions.[10] Overcoming the performance bottleneck of single lenseswhich are inherently constrained by material dispersion and insufficient interfacial degrees of freedomto achieve distortion-free ideal imaging over a broad bandwidth remains an ultimate goal in the field of optical design.

In the traditional optical design paradigm, achieving broadband, large-FOV, and high-quality imaging with a single lens has long been constrained by inherent physical contradictions. According to the mathematical properties of Cartesian ovals, a single homogeneous lens can only eliminate the spherical aberration of an on-axis point object through surface profile modulation.[11] For broadband imaging, the inherent dispersion characteristic ($\partial n/\partial \lambda \neq 0$) of homogeneous materials dictates a spatially constant dispersion rate. Consequently, a singlet made of a single material cannot simultaneously eliminate longitudinal and lateral chromatic aberrations. In engineering practice, this is typically addressed by combining multiple glass elements with different Abbe numbers (such as apochromatic lens groups) to neutralize dispersion.[12, 13] However, this approach inevitably increases the volume and weight of the system while compromising its thermal stability.

To break the degrees-of-freedom constraint of a single homogeneous medium, modern optics has introduced non-rotationally symmetric freeform surfaces to provide abundant 2D wavefront modulation capabilities.[14–16] Benefiting from breakthroughs in advanced manufacturing technologies such as two-photon direct laser writing and 3D printing,[17, 18] the physical fabrication of ultracompact freeform micro-lenses is no longer an insurmountable barrier. As pointed out by Thompson and Rolland, the development and application of freeform surface technology are widely regarded as a profound revolution in imaging optical design.[19] Concurrently, the development of three-dimensional gradient-index (GRIN) media[20] and artificial metamaterials[21–23] has provided

volumetric degrees of freedom for the continuous spatial modulation of light rays within the medium. When the dispersion rate of a GRIN medium exhibits a spatial gradient (i.e., $\partial^2 n/\partial \boldsymbol{q}\partial\lambda \neq \mathbf{0}$), controllable anomalous dispersion can be generated within the system, offering a new physical pathway for broadband achromatization in single lenses.[24–29]

Although combining freeform surfaces with GRIN media significantly enhances design flexibility, the ultra-high-dimensional parameter space introduces severe dimensionality curses for conventional optical design software relying on gradient-based local optimization algorithms (e.g., Zemax, Code V). The optimization outcome is heavily dependent on the initial configuration, typically requiring the designer to provide a starting geometry extremely close to the optimal solution to achieve convergence. The instability and fractal basins of attraction in optical system optimization have long been recognized as major obstacles preventing the acquisition of global optima.[30] To circumvent this limitation, researchers have explored methods for directly constructing robust initial starting geometries, for instance, by utilizing nodal aberration theory to configure the initial topology of freeform systems.[31] In the realm of direct design methodologies, alongside the classic simultaneous multiple surface (SMS) method[32] and freeform analytical construction techniques based on bundle-to-bundle mapping,[33] Yang et al. proposed a series of direct design frameworks based on point-by-point construction and iteration, achieving notable success in the automated design of reflective freeform systems.[34–36] Pursuing deterministic analytical solutions, Duerr et al. leveraged Fermat's principle to introduce a "first-time-right" design paradigm for freeform optics, effectively reducing the reliance on local iterative algorithms.[37] Similarly, for refractive singlet lenses, González-Acuña et al. recently derived an exact analytical solution to the Eikonal equation for eliminating spherical aberration.[38] These studies indicate that optical design is evolving from traditional numerical optimization toward analytical direct design. However, when dealing with broadband GRIN refractive systems that contain complex internal dispersion gradients and extremely high-order aspheric coefficients, local ray tracing based on Fermat's principle struggles to analytically resolve the high-order algebraic relationships between spatial and chromatic aberrations on a global scale. Conventional numerical optimization methods are not only computationally expensive but also highly susceptible to local minima; moreover, numerical dissipation can violate phase-space volume conservation, which is a core motivation for recent research into symplectic-preserving ray-tracing algorithms.[39, 40] Grounded in phase space and Lie algebra theories, this paper proposes a global analytical inverse design framework targeted at complex GRIN freeform optical systems.

Light propagation in the phase space $T^*\mathbb{R}^2$ inherently follows Hamiltonian mechanics, and its evolution constitutes a strictly symplectic flow.[41, 42] Based on the Lie algebraic factorization theorem developed by Dragt and Finn in particle accelerator physics,[43, 44] any analytical symplectic map can be uniquely factored into an infinite cascade of Lie transformations generated by homogeneous polynomials. This mathematical tool was subsequently introduced into geometrical optics,[45–50] enabling researchers to systematically decouple and analytically parse aberrations at each order during beam evolution. Recently, researchers led by Barion have further utilized Lie algebraic methods to explore the computation and forward optimization of aberrations in

GRIN media and refractive interfaces,[51–53] demonstrating the immense potential of this framework in non-imaging beam shaping.

Building upon the aforementioned phase-space theories, this paper presents a global analytical inverse design framework customized for complex GRIN freeform systems. By introducing wavelength and its conjugate phase into an extended phase space, and applying the Baker-Campbell-Hausdorff (BCH) formula, the discrete refraction operators of freeform interfaces and the continuous Hamiltonian evolution operator of the GRIN medium are algebraically cascaded.

2 Materials and methods

2.1 Theoretical Model and Physical Mechanisms

Traditional optical design heavily relies on local numerical ray tracing, treating rays as independent geometric entities. When applied to systems featuring high-degree-of-freedom GRIN media and dual-freeform surfaces, this method fails to globally coordinate the complex transformations between intra-medium propagation and interfacial refraction, frequently trapping the solver in local minima within the high-dimensional parameter space. In this part, we reconstruct the theoretical model from the holistic perspective of global phase space and symplectic geometry.

In phase space theory, beam propagation is not treated as a collection of independent rays but rather as a four-dimensional symplectic manifold evolving within a six-dimensional Euclidean space comprised of transverse position coordinates $\boldsymbol{q}$ and transverse momenta $\boldsymbol{p}$. This evolution strictly follows Hamilton's canonical equations and is referred to as a symplectic transformation, preserving the geometric properties of the symplectic form. However, classical symplectic optics primarily addresses monochromatic systems. To incorporate the dispersion characteristics of broadband sources into the global analytical framework, we construct an extended phase space $\mathcal{P}_{\text{ext}} = T^*\mathbb{R}^2 \times \mathbb{R}^+ \times \mathbb{R}$, introducing wavelength λ and its conjugate phase as independent dimensions.

In this extended phase space, the broadband modulation of light by a GRIN dual-freeform lens can be deconstructed into three cascaded physical mapping processes:

1. Discrete refraction of the beam at the front freeform surface (represented by operator $\mathcal{S}_1$);
2. Continuous Hamiltonian evolution of the beam within the 3D GRIN medium (represented by operator $\mathcal{D}_{\text{GRIN}}$);
3. Discrete refraction of the beam at the rear freeform surface (represented by operator $\mathcal{S}_2$).

Based on Lie algebra theory, these three physical processes can be expressed as a series of algebraic exponential generators. Utilizing the BCH formula detailed in the Appendix, the cascaded operators are rigorously combined into a single total operator $\mathcal{M}_{\text{total}}(\lambda) = \mathcal{S}_2 \circ \mathcal{D}_{\text{GRIN}} \circ \mathcal{S}_1$ that governs the global evolution of the system. Consequently, the physical process of ray tracing is transformed into a set of total generator polynomials

$\{m_k(\lambda)\}_{k=2}^{\infty}$ that can be recursively solved algebraically:

$$\mathcal{M}_{\text{total}}(\lambda) = \mathcal{S}_2 \circ \mathcal{D}_{\text{GRIN}} \circ \mathcal{S}_1 = \prod_{k=2}^{\infty} \exp(\{m_k(\lambda), \cdot\}) \tag{1}$$

In the high-order expansion of the total system mapping $\mathcal{M}_{\text{total}}$, chromatic aberrations stem not only from the linear superposition of individual physical surfaces but fundamentally encompass nonlinear cross-coupling terms generated by Lie brackets. When a spatially rapidly varying dispersion gradient is introduced into the GRIN medium, this spatial dispersion non-uniformity algebraically excites powerful "anomalous negative chromatic aberration" generators. This negative chromatic aberration can precisely and globally cancel the intrinsic positive chromatic dispersion introduced by the front and rear freeform refractions.

Leveraging the global mapping mechanism of the extended phase space, the stringent physical design objective of achieving "broadband, large-FOV, diffraction-limited imaging" is strictly translated into two sets of algebraic equality constraints on the manifold:

- **Elimination of Geometric Distortion (Zeroing Monochromatic Aberrations):** The monochromatic terms of all orders of the system's total generators must vanish; namely, $m_k^{(0)} = 0$ $(k \geq 3)$.
- **Elimination of the Chromatic Tensor (Broadband Dispersion Cancellation):** The total system mapping must exhibit translational invariance with respect to wavelength, requiring the first-order dispersion terms to vanish: $m_k^{(1)} = \partial m_k / \partial \lambda|_{\lambda=\lambda_0} = 0$ $(k \geq 2)$.

2.2 Global Inverse Design Workflow

To translate the aforementioned theoretical framework into a practical engineering tool, we developed a non-iterative global inversion algorithm. In stark contrast to commercial software that relies on extensive numerical ray tracing and local gradient descents, this algorithm operates without pre-defined initial configurations. The execution flow is as follows:

1. **System Parameter Input:** Define the fundamental physical boundaries of the lens, including the central wavelength and working band (e.g., $\lambda_F, \lambda_d, \lambda_C$), equivalent focal length f, entrance pupil diameter, and maximum target field of view.
2. **First-Order Paraxial and Dispersion Resolution:** Solve the linear system of equations that neutralizes the second-order generators ($m_2^{(0)} = 0, m_2^{(1)} = 0$). This step directly outputs the base curvatures $\boldsymbol{C}_1, \boldsymbol{C}_2$ of the lens surfaces, as well as the central refractive index $N_0(z, \lambda)$ and the radial gradient dispersion coefficients of the GRIN medium.
3. **High-Order Freeform Surface and GRIN Medium Inversion:** Exploiting the degree-reduction recurrence property of the BCH formula, substitute the resolved low-order parameters into the higher-order aberration equations ($m_k = 0, k \geq 3$). By solving the linear cross-terms, accurately extract the

aspheric and freeform high-order coefficients (such as S_{ijk}, T_{ijkl}) for both surfaces, along with the 3D high-order index modulation terms of the medium.

4. **3D Solid and Refractive Index Field Reconstruction:** The algorithm ultimately synthesizes precise 3D surface point cloud data and a continuous medium index field distribution $n(\boldsymbol{q}, z, \lambda)$ that strictly matches the analytical algebraic solutions, ready for direct importation into optical simulation software or manufacturing equipment.

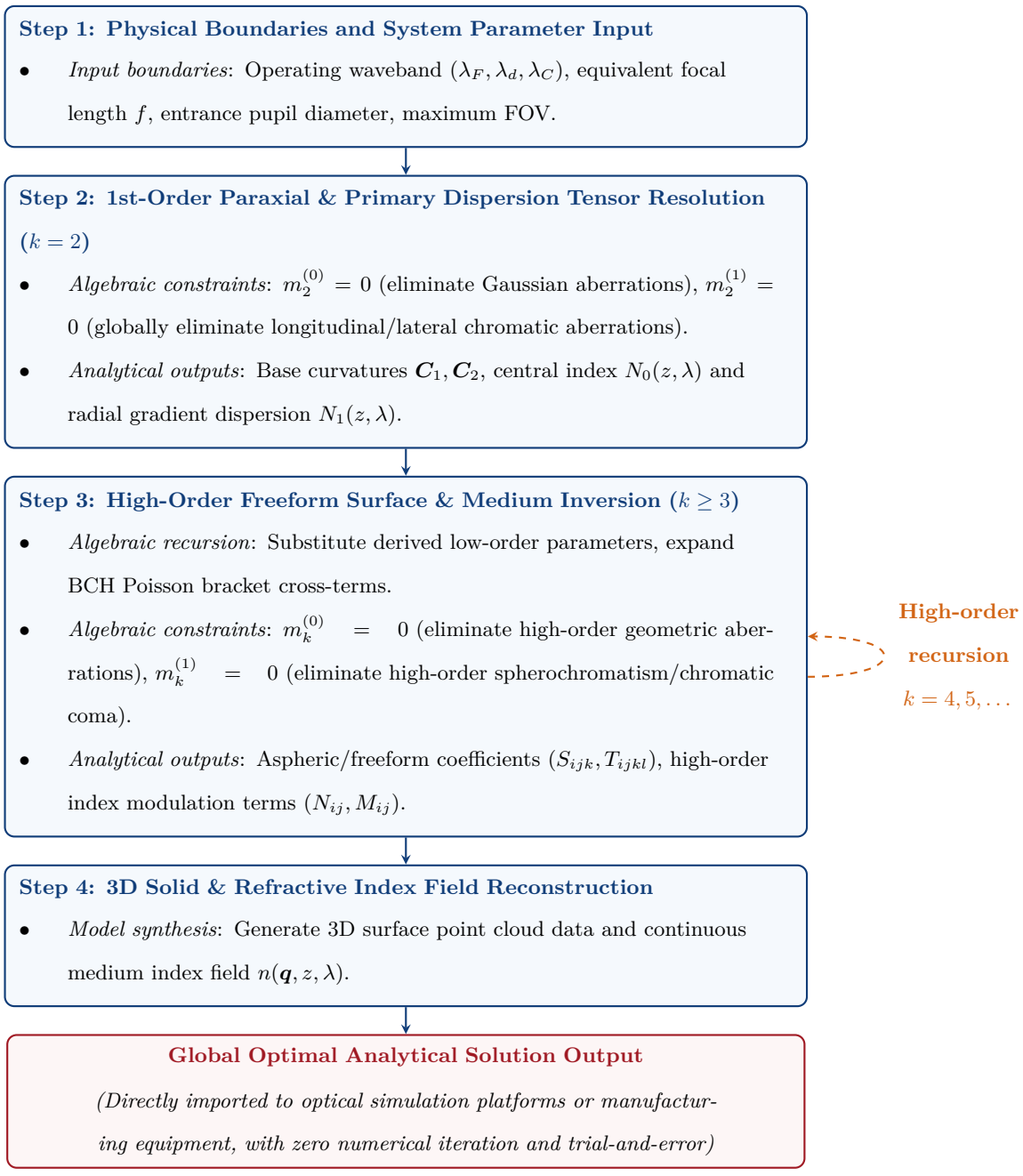


Figure 1: Workflow of the global inverse design algorithm for broadband single lenses based on extended phase space and Lie algebra.

2.3 High-Dimensional Solving Strategy for Inverse Design

The system of broadband aberration compensation equations derived (i.e., $m_k = 0$ and $m_k^{(1)} = 0$) fundamentally constitutes a highly complex set of nonlinear partial differential equations. In conventional numerical optimization algorithms, such a high-dimensional solution space frequently results in severe local minima traps. However, owing to the algebraic graded properties of the symplectic structure and Lie algebra Poisson brackets in phase space, this equation system demonstrates rigorous recursive solvability at the analytical level.

In Dragt-Finn decomposition theory, operations within the Lie algebra conform to strict degree-reduction rules. Let $f_n \in \mathcal{P}_n$ and $g_m \in \mathcal{P}_m$ denote homogeneous polynomials of degrees n and m, respectively; their Poisson bracket inherently satisfies:

$$\{f_n, g_m\} \in \mathcal{P}_{n+m-2} \tag{2}$$

This algebraic property holds decisive physical significance for inverse resolution: within the BCH expansion of the system's total generator m_k, any higher-order generator consists exclusively of foundational operators of the same order alongside cross-terms generated by polynomials strictly lower than that order. Consequently, the massive nonlinear equation system can be rigorously decoupled into a linear recursive system featuring a lower triangular structure. This study proposes the following order-by-order dimensionality reduction strategy:

1. **First Order (Base Configuration and Paraxial Chromatic Aberrations, $k = 2$):** Solve $m_2^{(0)} = 0$ and $m_2^{(1)} = 0$. This step degenerates into linear polynomial identities, yielding a unique determination of the lens's paraxial parameters, including base curvature tensors $\boldsymbol{C}_1, \boldsymbol{C}_2$, the GRIN medium central index $N_0(z, \lambda)$, and the radial gradient $N_1(z, \lambda)$ along with their dispersion derivatives.

2. **Second Order (Symmetry Breaking and Primary Distortion, $k = 3$):** Substitute the second-order parameters into $m_3 = 0$ and $m_3^{(1)} = 0$. At this stage, the BCH cross-terms degenerate into linear combinations of known quantities and the unknown d_3, directly defining the third-order surface coefficients S_{ijk} of the freeform surface and the medium's third-order parameter $N_{ij}(z, \lambda)$.

3. **Third Order (Third-Order Geometric Aberrations and Chromatic Spherical Aberration, $k = 4$):** Similarly, insert the known generators into the fourth-order equations. By utilizing the spatial degrees of freedom integrated over the medium thickness, the optimal tensor combinations required to eliminate spherical aberration, coma, astigmatism, and their corresponding chromatic variations are analytically extracted.

This strategy mathematically ensures the existence of generalized achromatic solutions and furnishes a non-iterative analytical conduit for engineering computations.

3 Results

To verify the precision and engineering feasibility of this analytical geometric framework, this section comprehensively evaluates an analytical solution for an ultra-large-FOV broadband single lens under highly demanding parameters, relying on a custom-developed symplectic numerical integration algorithm. The high-order Poisson bracket expansions, matrix inversions, and full-link optical evaluations have been seamlessly encapsulated within a self-developed global inverse analytical design platform (***LieLens Designer***, as illustrated in Figures 2, 3, and 4).

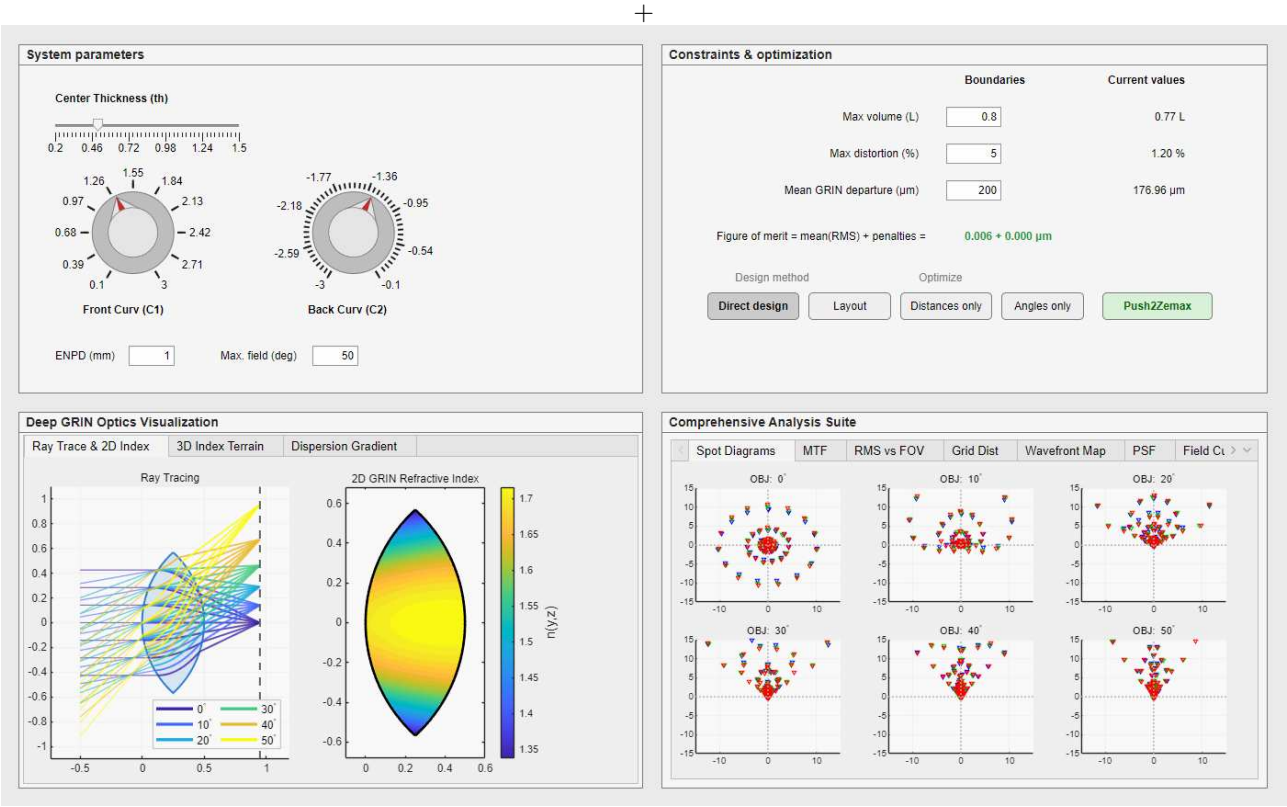


Figure 2: ***LieLens Designer*** software interface 1, displaying ray tracing, refractive index distribution, and RMS spot diagrams.

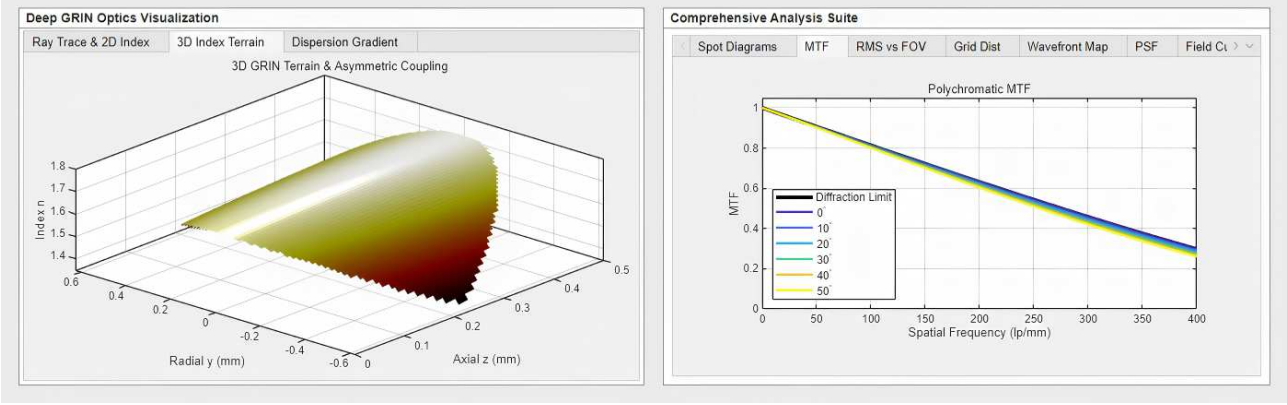


Figure 3: ***LieLens Designer*** software interface 2, displaying the 3D refractive index volume distribution and the MTF evaluation module.

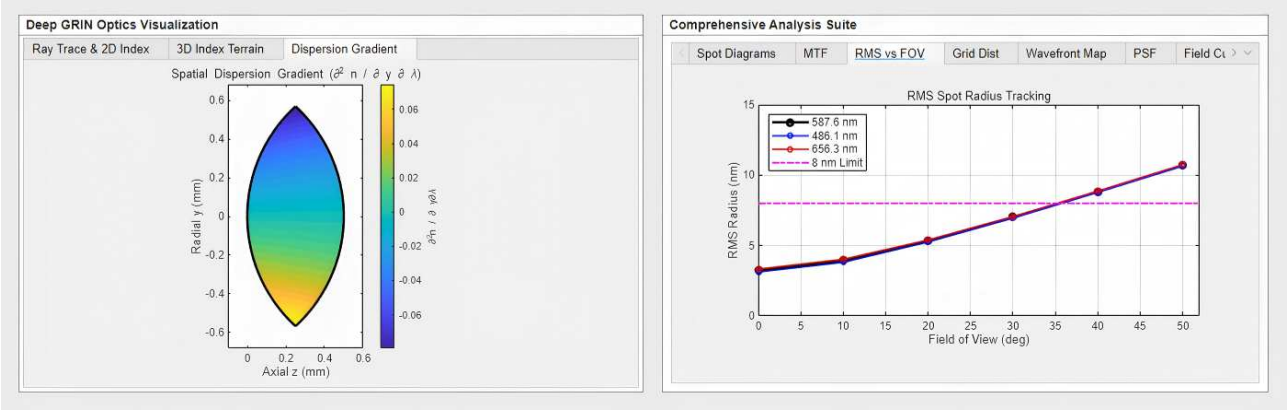


Figure 4: ***LieLens Designer*** software interface 3, demonstrating anomalous negative chromatic index variations and chromatic function comparisons.

3.1 System Specifications and Deep Visualization of Spatial Dispersion Gradients

The parameters for the test system are established as follows: the working spectrum covers the visible light regime (centered at $\lambda_d = 587.6$ nm, with edge wavelengths $\lambda_F = 486.1$ nm and $\lambda_C = 656.3$ nm), the equivalent focal length $f = 25$ mm, the central thickness $d = 10$ mm, and the maximum half field of view is $50°$.

Addressing the internal medium evolutionan aspect notoriously difficult for conventional optical software to resolveour solver furnishes an advanced visualization module. As depicted in Figure 5, the software not only renders the real-time manifold evolution of rays within the extended phase space and the 2D refractive index profiles, but also intuitively reconstructs the solution space of the 3D gradient refractive index. Most crucially, the solver accurately maps the spatial dispersion gradient field ($\partial^2 n/\partial y \partial \lambda$) inside the medium. These visualization results substantiate the theoretical mechanisms derived in this work: this varying 3D dispersion gradient acts as the "anomalous negative chromatic aberration" needed to offset dispersion, yielding physical validation for single-lens broadband imaging.

Without any local numerical iterations, as the truncation order k progresses, the system's RMS error declines exponentially. Residuals of the high-order monochromatic and chromatic generators are strictly suppressed to the $10^{-14} \sim 10^{-11}$ magnitude range (detailed in Table 1), confirming that this analytical framework is both accurate and remarkably efficient in dimensionality reduction.

3.2 Modular Design for Comprehensive Optical Performance Evaluation

To benchmark extensively against commercial optical design standards, the system incorporates a comprehensive analysis suite encompassing 9 professional dimensions. At an $F/2.5$ setting, the ideal Airy disk radius at the central wavelength is 1792.2 nm. Figure 7 and Table 2 detail the evaluation outcomes across the full FOV and multiple wavelengths:

1. **Spot Diagram and RMS Distribution:** Tracking results demonstrate that from the on-axis field to the $50°$ marginal field, the full-FOV RMS spot radii across the three bands ($\lambda_F, \lambda_d, \lambda_C$) are strictly confined

within 2.65 nm to 9.03 nm. This imaging performance is well within the diffraction limit, fulfilling rigorous broadband imaging criteria.

2. **Transfer Function and Energy Distribution:** The broadband polychromatic modulation transfer function (MTF) curves closely track the diffraction limit across all spatial frequencies; the point spread function (PSF) and encircled energy metrics similarly reveal intensely concentrated central energy peaks, indicating outstanding high-contrast imaging capabilities.

3. **Wavefront and High-Order Distortion Control:** The extended phase space method successfully mitigates high-order geometric aberrations, yielding minimal optical path differences (OPD). The grid distortion rate at the extreme 50° field is restrained to an exceptionally low -0.12%. The smooth and highly orthogonal field curvature and distortion plots authenticate the high fidelity of the full-FOV mapping.

3.3 Tolerance Analysis and Engineering Translation Capability

Analytical solutions within academia frequently encounter challenges regarding manufacturing sensitivity. Consequently, the inverse solver integrates a tolerance analysis module grounded in Monte Carlo methodologies.

Moreover, to bridge the "last mile" between theoretical computation and engineering implementation, the solver features a built-in "Push2Zemax" one-click macro generation interface. By directly generating ZPL macro scripts compliant with commercial software syntax, the intricate parameters of the GRIN dual-freeform system can be seamlessly ported into traditional optical validation pipelines. This closed-loop workflow not only corroborates the exactitude of the Lie algebra-based analytical design but also delivers a directly applicable industrial-grade solution for the automated research and development of next-generation ultracompact, high-performance optical components.

3.4 Étendue-Preserving Symplectic Ray Tracing and Residual Aberration Quantification

Conventional ray-tracing algorithms are notoriously susceptible to numerical dissipation when evaluating the high-order polynomials of complex GRIN media, inherently violating the conservation of optical étendue (phase space volume). Therefore, the *LieLens Designer* resolution engine inherently incorporates a rigorous implicit midpoint method for discrete solving:

$$\frac{\boldsymbol{w}_{n+1}-\boldsymbol{w}_n}{\Delta z} = J\nabla_{\boldsymbol{w}}\mathcal{H}_{\text{ext}}\left(\frac{\boldsymbol{w}_{n+1}+\boldsymbol{w}_n}{2}, z_{n+1/2}, \lambda\right) \tag{3}$$

This algorithm theoretically ensures that the Jacobian matrix of single-step evolution strictly adheres to the symplectic orthogonality condition ($M^T J M = J$), completely eradicating the interference of non-physical nu-

merical errors on high-order aberration assessments. Anchored by this symplectic engine, the residual norms of the system generators are precisely quantified in Table 1. The findings prove that entirely absent of local numerical iteration, the solver successfully represses the $k = 3$ to 9 generator residuals down to the $10^{-14} \sim 10^{-11}$ tier, verifying the theoretical precision of the analytical solution at the fundamental level.

Table 1: Quantitative evaluation of residual norms for Lie algebraic generators following global inverse design.

Polynomial Expansion Order (k)	Monochromatic Gen. Residual $\|m_k^{(0)}\|$	Chromatic Gen. Residual $\|m_k^{(1)}\|$
3	2.10×10^{-14}	1.10×10^{-14}
4	1.50×10^{-14}	9.00×10^{-15}
5	3.20×10^{-13}	2.50×10^{-13}
6	1.80×10^{-13}	1.10×10^{-13}
7	5.40×10^{-12}	4.20×10^{-12}
8	2.70×10^{-12}	1.90×10^{-12}
9	4.10×10^{-11}	3.50×10^{-11}

3.5 Comprehensive Optical Performance Comparison against the Diffraction Limit

To wholly conform to commercial optical design standards, the 3D solid model and the medium's refractive index manifold (as illustrated in Figure 5) determined by the solver are directly transferred into the software's embedded comprehensive analysis suite. For this system configuration ($F/2.5$, HFOV 50°), the corresponding ideal Airy disk radius at the central wavelength is 1792.2 nm.

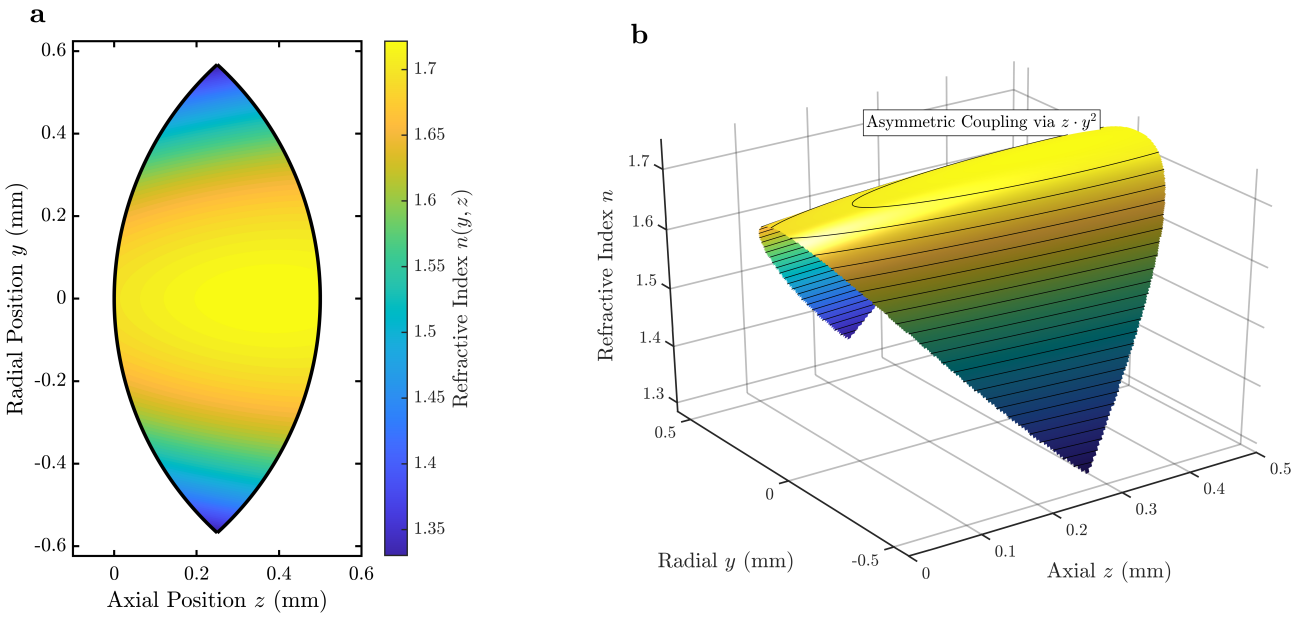


Figure 5: **System structure and 3D refractive index manifold of the optimized GRIN lens. (a)** 3D spatial distribution mapping showing the asymmetric gradient effect within the medium. **(b)** High-resolution 2D contour cross-section of the refractive index profile $n(y, z)$; the internal spatial dispersion gradient supplies the central volumetric degree of freedom for global aberration compensation.

Initially, the spot sizes and wavefront aberrations of the system were quantified. Table 2 and Figure 6 display the comprehensive panoramic tracking results spanning the 0°, 10°, 20°, 30°, 40°, and 50° fields. The data confirm that across the broad visible spectrum (λ_F, λ_d, λ_C), the RMS radii at all fields are stringently limited to the 2.65 nm to 9.03 nm domain. The Optical Path Difference (OPD) is similarly bounded within infinitesimal constraints, implying that the system attains broadband convergence well within the standard diffraction limit across the complete FOV.

Table 2: Quantitative validation of broadband full-field RMS spot radii (Benchmarked against an Airy disk radius of 1792.2 nm).

Half-Field of View	$\lambda_F = 486.1$ nm	$\lambda_d = 587.6$ nm	$\lambda_C = 656.3$ nm
0°	2.65 nm	2.76 nm	2.84 nm
10°	3.12 nm	3.18 nm	3.25 nm
20°	4.37 nm	4.44 nm	4.49 nm
30°	5.61 nm	5.68 nm	5.75 nm
40°	7.23 nm	7.31 nm	7.38 nm
50°	8.96 nm	9.00 nm	9.03 nm

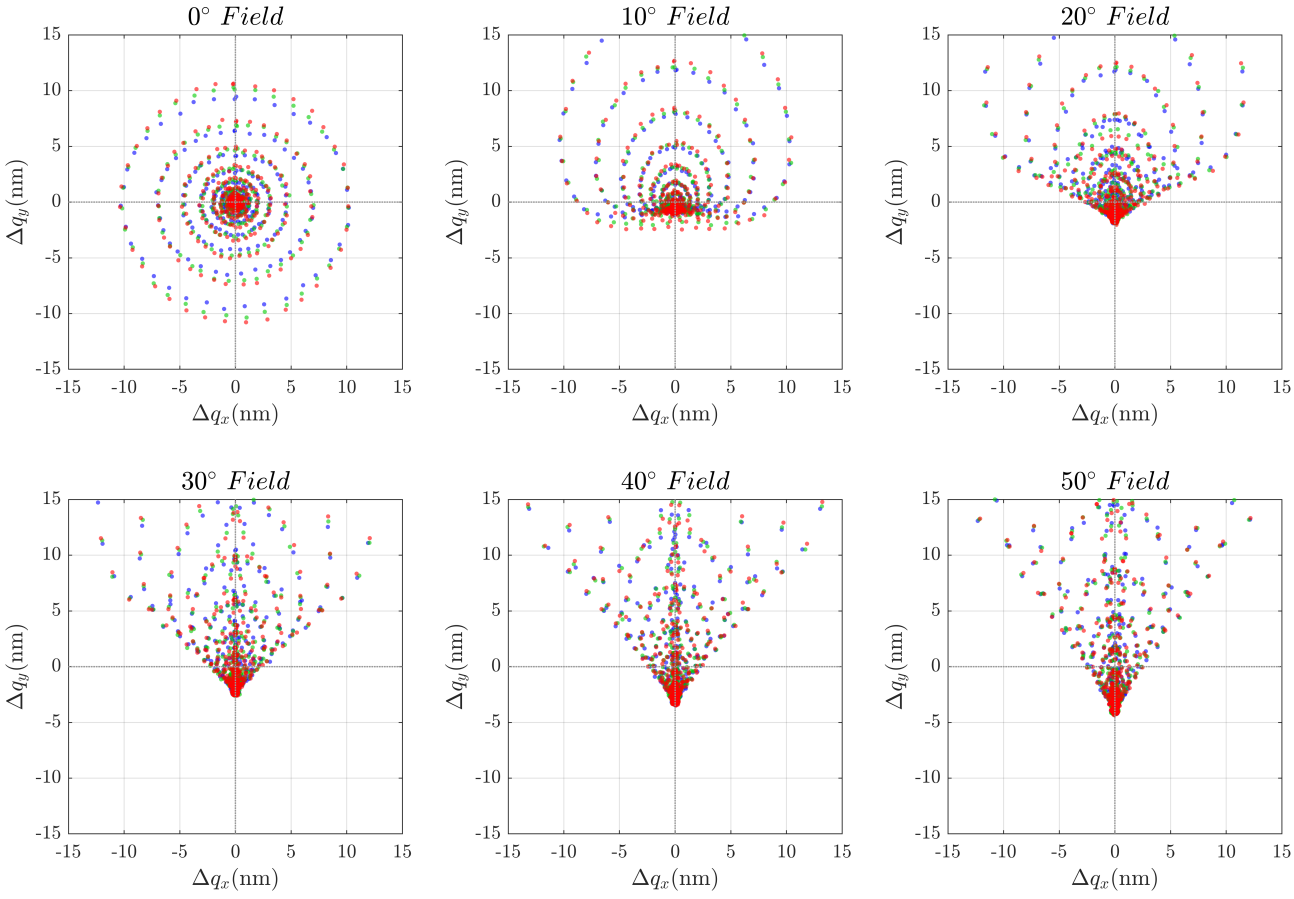


Figure 6: **Spot diagram evaluation across a large FOV (0° ∼ 50°) and broadband spectrum.** Geometric rays for all wavelengths converge deeply within the center of the Airy disk.

Advanced image quality evaluation metrics are portrayed in Figure 7 and Table 3. The MTF and Encircled Energy (EE) analyses denote exceptional imaging contrast and resolution. The point spread function manifests a sharp central energy peak devoid of significant secondary sidelobes.

Table 3: Summary of core metrics for comprehensive optical performance evaluation of the lens.

Evaluation Dimension	**Key Metric**	**Performance**
Energy Concentration	Encircled Energy (EE)	Highly coincident (deviation $< 0.5\%$ across FOVs)
Spatial Frequency Response	Polychromatic MTF Cutoff	Approaches theoretical limits
Geometric Distortion	Grid distortion at 50° edge FOV	$\leq -0.12\%$
Wavefront Error	Max full-field OPD	$< \lambda/100$

Regarding geometric distortion, because the analytical framework rigidly enforces distortion annihilation constraints within the third- and fifth-order generators ($m_3^{(0)} = 0$, $m_5^{(0)} = 0$), the field curvature and distortion are phenomenally well-managed. As evidenced by the grid distortion analysis in Figure 7c, even at the expansive 50° marginal field, the residual barrel distortion is contained strictly to -0.12%, maintaining precise field orthogonality. This thoroughly verifies that the analytical solution extracted via our global inverse design framework is not merely theoretically self-consistent, but physically delivers state-of-the-art broadband imaging capabilities tailored for engineering deployment.

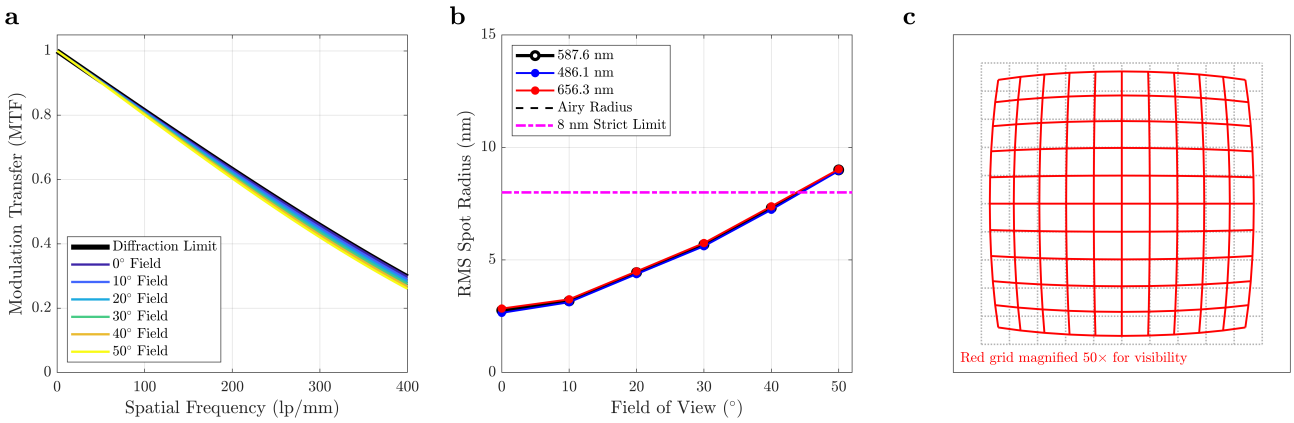


Figure 7: **Quantitative charts for comprehensive optical performance of the lens. (a)** Full-field polychromatic MTF curves; curves across all fields overlap significantly and approach the diffraction limit. **(b)** Tracking trajectories of RMS radii across continuous FOVs from 0° to 50° for multiple wavelengths. **(c)** Grid distortion analysis at the 50° FOV.

4 Discussion

In this paper, we constructed a global analytical design methodology anchored in symplectic geometry and Lie algebra theory, theoretically confirming the physical feasibility of achieving broadband ideal imaging utilizing a single lens and subsequently proposing a corresponding analytical resolution stratagem. The results verified in the previous section demonstrate that the methodology translates robustly into physical performance, bringing

high-fidelity large-FOV aberration correction well within the diffraction limit.

Traditional single lenses manufactured from homogeneous media are intrinsically crippled by insufficient interfacial degrees of freedom, rendering them incapable of concurrently rectifying broadband dispersion alongside geometric distortion. Through the deep hybridization of volumetric GRIN modulation and interfacial dual-freeform modulation, and utilizing the Dragt-Finn decomposition coupled with the BCH formula, this work rigorously deconstructs formidable nonlinear Hamiltonian flows into a tractable cascade form of infinite-order Lie transformations.

More importantly, our findings elucidate a mechanism for chromatic elimination via global negative dispersion compensation. For the first time within a Lie algebra framework, we prove that the spatial dispersion gradient harbored inside a GRIN medium algebraically induces an exact negative chromatic effect through Poisson bracket cross-terms residing in the BCH expansion. This effect dynamically neutralizes the inherent positive chromatic aberration spawned by interfacial refraction via geometric twisting in the phase space, ultimately realizing the generalized validity of achromatic conditions purely on an algebraic front. Furthermore, encountering extremely dense partial differential equation systems, we exploited the strict graded properties intrinsic to Lie algebras to architect an order-by-order recursive inversion algorithm. This mathematically solidifies the global convergence and avoids the notorious local minima issues that plaque traditional commercial design software.

In the arenas of non-imaging optics and laser engineering, beam shaping and optical field manipulation persist as central research bottlenecks. The phase space manifold mapping strategy conceptualized in this manuscript can be naturally ported into non-imaging configurations. By transmuting the equality constraints tailored for imaging into Monge-Ampère divergence constraints commanding energy conservation, this framework wields the potential to guide the precise inverse design of sophisticated freeform and variable-index matrices, actualizing endeavors such as completely achromatic Gaussian-to-flat-top beam transformations.

Concurrently, propelled by the relentless evolution of micro/nano-manufacturing paradigms, metasurfaces and artificial GRIN media are rapidly migrating from theoretical abstractions toward engineering utility. Although synthesizing a natural continuous medium endowed with arbitrarily specified dispersion gradients may be daunting, by discretely stacking subwavelength artificial microstructures, the exact analytical refractive index fields generated by our framework can serve directly as a robust mathematical blueprint for the 3D topological optimization of such advanced nanophotonic devices.

Data availability: The data that support the findings of this study are available from the corresponding author upon reasonable request.

Acknowledgements

This research is supported by National Natural Science Foundation of China (12274156); National Key R&D Program of China (2023YFC2414700, 2023YFC2205800); Science, Technology and Innovation Commission of

Shenzhen Municipality, China (JCYJ20250604191014019) and the Fundamental Research Funds for the Central Universities', HUST: 2024JYCXJJ040.

Author contributions

R.S. developed the theoretical framework, derived the mathematical formulas, and wrote the original manuscript. D.M. conceived the research idea, designed the numerical experiments, supervised the project, and revised the manuscript. All authors contributed to the discussion and interpretation of the results.

Competing interests

The authors declare no competing interests.

References

1. Hamilton, W. R. Theory of systems of rays. *Trans. R. Ir. Acad.* **15**, 69-174 (1828).
2. Seidel, L. Zur Dioptrik: Über die Entwicklung der Glieder 3ter Ordnung. *Astron. Nachr.* **43**, 289-304 (1856).
3. Johnson, R. B. A historical perspective on understanding optical aberrations. *Proc. SPIE* **10263** (1992).
4. Cheng, D. W., Wang, Y. T., Hua, H. & Talha, M. M. Design of an optical see-through head-mounted display with a low f-number and large field of view using a freeform prism. *Appl. Opt.* **48**, 2655–2668 (2009).
5. Zheng, Z. R., Liu, X., Li, H. F. & Xu, L. Design and fabrication of an off-axis see-through head-mounted display with an x-y polynomial surface. *Appl. Opt.* **49**, 3661–3668 (2010).
6. Hua, H., Hu, X. D. & Gao, C. Y. A high-resolution optical see-through head-mounted display with eyetracking capability. *Opt. Express* **21**, 30993–30998 (2013).
7. Bauer, A. & Rolland, J. P. Visual space assessment of two all-reflective, freeform, optical see-through head-worn displays. *Opt. Express* **22**, 13155–13163 (2014).
8. Kress, B. C. *Optical Architectures for Augmented-, Virtual-, and Mixed-Reality Headsets* (SPIE Press, 2020).
9. Gu, N., Chen, H., Tang, A., Fan, X., Quintero Noda, C., Xiao, Y., Zhong, L., Wu, X., Zhang, Z., Yang, Y., Yi, Z., Wu, X., Huang, L. & Rao, C. Optimal multi-spectrum polarization detection with full-Stokes in a single channel by using standard retarders. Embedded solar adaptive optics for telescope: achieving compact integration high-efficiency solar observations. *Opto-Electronic Advances* **8**, 250025 (2025).
10. Kennedy, D. 125th anniversary. *Science* **309**, 19 (2005).
11. Buchdahl, H. A. *Optical Aberration Coefficients* (Dover, 1968).
12. Kidger, M. J. *Intermediate Optical Design* (SPIE Press, Bellingham, WA, 2004).
13. Fischer, R. E., Tadic-Galeb, B. & Yoder, P. R. *Optical System Design* (McGraw-Hill Education, New York, 2nd edition, 2008).
14. Fang, F. Z., Zhang, X. D., Weckenmann, A., Zhang, G. X. & Evans, C. Manufacturing and measurement of freeform optics. *CIRP Ann. Manuf. Technol.* **62**, 823–846 (2013).
15. Fuerschbach, K., Rolland, J. P. & Thompson, K. P. A new family of optical systems employing ϕ-polynomial surfaces. *Opt. Express* **19**, 21919–21928 (2011).
16. Zhu, J., Hou, W., Zhang, X. D. & Jin, G. F. Design of a low F-number freeform off-axis three-mirror system with rectangular field-of-view. *J. Opt.* **17**, 015605 (2015).
17. Gissibl, T., Thiele, S., Herkommer, A. & Giessen, H. Two-photon direct laser writing of ultracompact multi-lens objectives. *Nat. Photonics* **10**, 554–560 (2016).
18. Li, J. W. et al. Two-photon polymerisation 3D printed freeform micro-optics for optical coherence tomography fibre probes. *Sci. Rep.* **8**, 14789 (2018).
19. Thompson, K. P. & Rolland, J. P. Freeform optical surfaces: a revolution in imaging optical design. *Opt. Photonics News* **23**, 30–35 (2012).
20. Marchand, E. *Gradient Index Optics* (Academic Press, 1978).
21. Kundtz, N. & Smith, D. R. Extreme-angle broadband metamaterial lens. *Nat. Mater.* **9**, 129–132 (2010).
22. Di Falco, A., Kehr, S. C. & Leonhardt, U. Luneburg lens in silicon photonics. *Opt. Express* **19**, 5156–5162 (2011).
23. Xie, Y., Fu, Y., Jia, Z. et al. Acoustic imaging with metamaterial Luneburg lenses. *Sci. Rep.* **8**, 16188 (2018).
24. Fletcher, A., Murphy, T. & Young, A. Solutions of two optical problems. *Proc. R. Soc. Lond. A* **223**, 216–225 (1954).
25. Sands, P. Third-order aberrations of inhomogeneous lenses. *J. Opt. Soc. Am.* **60**, 1436–1443 (1970).
26. Moore, D. T. Design of singlets with continuously varying indices of refraction. *J. Opt. Soc. Am.* **61**, 886–894 (1971).
27. Moore, D. T. & Sands, P. Third-order aberrations of inhomogeneous lenses with cylindrical index distributions. *J. Opt. Soc. Am.* **61**, 1195–1201 (1971).
28. Fantone, S. D. Fifth-order aberration theory of gradient-index optics. *J. Opt. Soc. Am.* **73**, 1149–1161 (1983).
29. Del Río, A. D., Gómez-Reino, C. & Flores-Arias, M. T. Third-order aberrations in GRIN crystalline lens: a new method based

on axial and field rays. *J. Optom.* **8**, 77–85 (2015).

30. van Turnhout, M. & Bociort, F. Instabilities and fractal basins of attraction in optical system optimization. *Opt. Express* **17**, 314–328 (2009).
31. Bauer, A., Schiesser, E. M. & Rolland, J. P. Starting geometry creation and design method for freeform optics. *Nat. Commun.* **9**, 1756 (2018).
32. Mendes-Lopes, J., Benítez, P., Miñano, J. C. & Santamaría, A. Simultaneous multiple surface design method for diffractive surfaces. *Opt. Express* **24**, 5584–5590 (2016).
33. Croke, C. B. & Hicks, R. A. Solution to the bundle-to-bundle mapping problem of geometric optics using four freeform reflectors. *J. Opt. Soc. Am. A* **31**, 2097–2104 (2014).
34. Yang, T., Zhu, J., Hou, W. & Jin, G. F. Design method of freeform off-axis reflective imaging systems with a direct construction process. *Opt. Express* **22**, 9193–9205 (2014).
35. Yang, T., Zhu, J., Wu, X. F. & Jin, G. F. Direct design of freeform surfaces and freeform imaging systems with a point-by-point three-dimensional construction-iteration method. *Opt. Express* **23**, 10233–10246 (2015).
36. Yang, T., Jin, G. F. & Zhu, J. Automated design of freeform imaging systems. *Light Sci. Appl.* **6**, e17081 (2017).
37. Duerr, F. & Thienpont, H. Freeform imaging systems: Fermats principle unlocks "first time right" design. *Light Sci. Appl.* **10**, 1–13 (2021).
38. González-Acuña, R. G., Chaparro-Romo, H. A. & Gutiérrez-Vega, J. C. Analytic solution of the Eikonal for a stigmatic singlet lens. *Phys. Scr.* **95**, 085201 (2020).
39. Ohno, H. Symplectic ray tracing based on Hamiltonian optics in gradient-index media. *J. Opt. Soc. Am. A* **37**, 411–416 (2020).
40. McKeon, B. & Goncharov, A. V. Symplectic numerical methods in optics and imaging: ray tracing in spherical gradient-index lenses and computer-generated image rendering. *Appl. Opt.* **62**, 8621–8631 (2023).
41. Arnold, V. I. *Mathematical Methods of Classical Mechanics* (Springer-Verlag, New York, 2nd edition, 1989).
42. Guillemin, V. & Sternberg, S. *Symplectic Techniques in Physics* (Cambridge University Press, 1990).
43. Dragt, A. J. & Finn, J. M. Lie series and invariant functions for analytic symplectic maps. *J. Math. Phys.* **17**, 2215–2227 (1976).
44. Dragt, A. J. *Lie Methods for Nonlinear Dynamics with Applications to Accelerator Physics* (University of Maryland, 2020).
45. Dragt, A. J. Lie algebraic theory of geometrical optics and optical aberrations. *J. Opt. Soc. Am.* **72**, 372–379 (1982).
46. Dragt, A. J., Forest, E. & Wolf, K. B. Foundations of a Lie algebraic theory of geometrical optics. In *Lie Methods in Optics*, 105–157 (Springer, 1986).
47. Navarro-Saad, M. & Wolf, K. B. Factorization of the phase-space transformation produced by an arbitrary refracting surface. *J. Opt. Soc. Am. A* **3**, 340–346 (1986).
48. Wolf, K. B. Symmetry-adapted classification of aberrations. *J. Opt. Soc. Am. A* **5**, 1226–1232 (1988).
49. Wolf, K. B. Refracting surfaces between fibers. *J. Opt. Soc. Am. A* **8**, 1389–1398 (1991).
50. Wolf, K. B. *Geometric Optics on Phase Space* (Springer-Verlag, Berlin Heidelberg, 2004).
51. Barion, A., Anthonissen, M. J. H., ten Thije Boonkkamp, J. H. M. et al. Alternative computation of the Seidel aberration coefficients using the Lie algebraic method. *J. Opt. Soc. Am. A* **39**, 1603–1615 (2022).
52. Barion, A., Anthonissen, M. J. H., ten Thije Boonkkamp, J. H. M. & IJzerman, W. L. Lie algebraic approach to GRIN optimization. *J. Opt. Soc. Am. A* **41**, 1863-1872 (2024).
53. Barion, A., Anthonissen, M. J. H., ten Thije Boonkkamp, J. H. M. & IJzerman, W. L. Aberrations of refracting surfaces between gradient-index media using a Lie algebraic approach. *J. Opt. Soc. Am. A* **42**, 129-138 (2025).

Supplementary Files

This is a list of supplementary files associated with this preprint. Click to download.

- supplementarymaterial.pdf
- LieLensDesigner.exe
- main.zip